

High-pressure and high-temperature multianvil synthesis of metastable polymorphs of Bi_2O_3 : Crystal structure and electronic properties

S. Ghedia, T. Locherer, R. Dinnebier, D. L. V. K. Prasad, U. Wedig, and M. Jansen
Max Planck Institute for Solid State Research, Heisenbergstrasse 1, D-70569 Stuttgart, Germany

A. Senyshyn
Institute for Materials Science, Darmstadt University of Technology, D-64287 Darmstadt, Germany
and Forschungsneutronenquelle Heinz Maier-Leibnitz, Technische Universität München, D-85747 Garching b. München, Germany
 (Received 21 June 2010; published 23 July 2010)

High-pressure and high-temperature experiments with Bi_2O_3 using a 6–8 type multianvil device led to the formation of a metastable polymorph (HP- Bi_2O_3) with noncentrosymmetric trigonal symmetry. This phase relaxes during the course of several months at ambient temperature or more rapidly via annealing, to a second intermediate modification (R- Bi_2O_3). Upon further annealing finally the transformation back to the known ambient phase (α - Bi_2O_3) takes place. Both crystal structures were solved from high-resolution x-ray and neutron powder-diffraction data. The orientation and stereochemical activity of the Bi^{3+} lone pairs (or inert pairs) is discussed in terms of crystal-chemical considerations and density-functional theory calculations. Whenever suitable, results were verified by experimental determination of the respective properties. The results of the theoretical analyses show that within the structure type of HP- Bi_2O_3 , bismuth oxide exhibits a pronounced polarization and can be considered as ferroelectric.

DOI: [10.1103/PhysRevB.82.024106](https://doi.org/10.1103/PhysRevB.82.024106)

PACS number(s): 61.66.–f, 71.20.–b

I. INTRODUCTION

Many binary oxides and fluorides of the heavier group 13–16 elements have remained unexplored at high-pressure and high-temperature conditions. When the respective cation occurs in the lower oxidation state (i.e., $N-2$, where N = group number) it retains a lone electron pair, which often exhibits stereochemical activity leading to distorted crystal structures. The importance of such lone pairs in structural chemistry has been discussed extensively and attempts were made at describing the various coordination polyhedra observed for the lone pair bearing cations.^{1,2} In particular, the volume occupied by the lone pair was approximated to that of an oxygen atom.³ In recent times lone pair containing compounds in general have attracted increasing attention due to their unique crystal structures, which may be characterized by hollow cavities⁴ or layers⁵ and give rise to physical properties such as ferroelectricity⁶ or piezoelectricity.⁷ Reports as to the response of such lone-pair compounds to high pressure are still limited but include a few experimental investigations, e.g., on SnO ,⁸ PbO ,^{9–11} and Pb_3O_4 (Ref. 12) as well as theoretical studies, e.g., dealing with TlF (Ref. 13) or TlI, InBr, and InI.¹⁴ When considering the response of the lone pairs under high pressure, several scenarios can be envisaged. On the one hand the lone pairs could be forced into a pure s -type state, becoming stereochemically inactive. As another effect under high pressure the valence band (in most instances containing the lone pairs) and the conduction band broaden and might overlap, leading to semiconducting or metallic behavior, respectively.¹⁵ Finally, in mixed valence lone-pair compounds it is possible that the lone pairs delocalize (rendering the valence states of the respective cations indiscernible), yielding a partially filled band at the Fermi level and inducing metallic behavior.¹⁶ The relatively large amount of empty space available in the crystal structures of

lone-pair compounds is what makes them particularly suited to high-pressure and high-temperature investigations since under these conditions a polymorphic transition to a denser phase (perhaps with elevated coordination of the cations) is expected to occur, which may persist in a metastable state at ambient pressure and temperature as it was found for SeO_2 .¹⁷ One interesting candidate for such high-pressure and high-temperature investigation is bismuth(III) oxide, which represents one of the industrially most important compounds of bismuth. It is a pale yellow, crystalline solid found naturally as the minerals bismite (monoclinic) and sphaerobismoite (tetragonal). In recent times it has attracted particular attention as a potential electrolyte for use in gas sensors or solid oxide fuel cells. At ambient conditions Bi_2O_3 crystallizes in the monoclinic space group $P2_1/c$. This represents its thermodynamically stable modification and is termed α - Bi_2O_3 . The crystal structure is composed of a three-dimensional (3D) network of corner- and edge-sharing distorted BiO_5 square pyramids.¹⁸ When heated above 729 °C, α - Bi_2O_3 transforms to cubic face-centered δ - Bi_2O_3 , which possesses a fluorite-type structure with statistically disordered oxygen vacancies and accordingly a high ionic conductivity (1 S cm^{-1} at 750 °C).¹⁹ Upon cooling δ - Bi_2O_3 two further phases can be obtained; tetragonal β - Bi_2O_3 at 650 °C (lower symmetry variant of δ - Bi_2O_3 with ordering of oxygen vacancies) and cubic body-centered γ - Bi_2O_3 at 639 °C (related to the $\text{Bi}_{12}\text{GeO}_{20}$ structure).²⁰ In addition to these four well-known polymorphs there are also more recent reports of a metastable polymorph prepared by hydrothermal treatment, ϵ - Bi_2O_3 , which (although the authors did not point out) crystallizes isotypic to orthorhombic Sb_2O_3 (valentinite), and was observed to transform irreversibly to α - Bi_2O_3 at 400 °C.²¹ Finally an obscure triclinic phase (denoted ω - Bi_2O_3) has been reported, prepared by heating a thin film to 800 °C on a BeO substrate but its crystal structure was

not determined.²² In contrast to “temperature,” the parameter “pressure” has received comparatively little attention in the Bi_2O_3 literature to date. Based on high-pressure spectroscopic studies of Bi_2O_3 up to 30 GPa in a diamond-anvil cell a transition to a metastable amorphous state at 21 GPa was claimed, however, no new crystalline phases were found.²³ To the best of knowledge only one report of a high-pressure phase of Bi_2O_3 has been made. In this a high-pressure and high-temperature investigation of Bi_2O_3 utilizing a DIA-6 type “large volume” press with graphite resistance heater was carried out, from which a metastable polymorph was obtained.²⁴ Synthesis of this high-pressure polymorph was carried out at a pressure of 6 GPa and a temperature of 880 °C. It was claimed that this modification is isotypic to the A- La_2O_3 structure type. Reliable analyses, such as Rietveld refinement of the powder x-ray data, were not provided. Presence of spurious reflections was mentioned, which the authors assigned to bismuth oxycarbonate originating from the graphite heater, entering the sample through cracks in the gold container. It was also pointed out that HP- Bi_2O_3 was kinetically unstable at ambient temperature with reflections appearing over time in the x-ray diffraction (XRD) patterns. However, no further studies were presented to account for these observations.

In order to settle the controversies and inconsistencies mentioned, we have performed further high-pressure and high-temperature experiments on Bi_2O_3 . As a result, we have identified two polymorphic modifications of bismuth(III) oxide and solved their crystal structures using x-ray and neutron powder diffraction. In order to investigate the electronic properties and phase stability of the high-pressure polymorphs, diffuse reflectance spectroscopy, and differential scanning calorimetry have also been applied. The results obtained were supported by density-functional theory (DFT) calculations. The chemical bonding properties and the stereochemical activities of the electron lone pairs are discussed on the basis of geometric models and DFT calculations as well.

II. EXPERIMENTAL

A. High-pressure and high-temperature experiments

For the high-pressure and high-temperature experiments high-purity Bi_2O_3 (Sigma-Aldrich, >99.999%) was employed. The material was preground and compacted into gold capsules (diameter: 4 mm). The experiments were carried out using a 6–8 type multianvil press (1000-Tonne, Max Voggenreiter GmbH, Mainleus, Germany) equipped with a Walker module. The sample capsules were loaded into $\text{MgO}/\text{Cr}_2\text{O}_3$ octahedra (edge length 25 mm) that were used in conjunction with 32 mm cubic tungsten carbide anvils (truncation length 15 mm). Sample pressure was determined on the basis of predetermined pressure/load calibration curves and sample heating accomplished via a LaCrO_3 resistance heater. Experimental conditions employed were typically $p=6.3$ GPa, $T=900$ °C, and $t=0.5$ h. Experiments were terminated by rapidly quenching the sample to ambient temperature and slow pressure release (15 h). In contrast to the pale yellow starting material the recovered Bi_2O_3 showed a much brighter yellow color.

B. Powder x-ray and neutron diffraction

High resolution x-ray powder-diffraction patterns of the HP and R phases of Bi_2O_3 were first collected at room temperature on a laboratory powder diffractometer [D8, Bruker, Cu $K\alpha 1$ radiation from primary Ge(111)-Johannson-type monochromator; LynxEye position sensitive detector with an opening angle of 3.5°] in Bragg-Brentano geometry with the samples loaded on a flat Si-(911) low background sample holder of 32 mm diameter by sprinkling the powder on a thin film of vacuum grease. The samples were aligned such to minimize sample height errors and rotated during measurement for better particle statistics. Data were generally taken in steps of 0.009° 2θ from 5.0°–90.0° 2θ with a total measurement time of 30 h each.

For high-resolution neutron powder-diffraction patterns of the HP and R phases of Bi_2O_3 the samples were placed in a vanadium can of 8 mm diameter and neutron data were recorded for 12 h at the structure powder diffractometer (SPODI) (Ref. 25) at FRM-II (Garching, Germany). At a monochromator takeoff angle of 155°, the Ge(551) monochromator yielded a wavelength of $\lambda = 1.5483$ Å. The wafer-stack monochromator consists of 17 Ge(551) crystals with mosaicities of 20' in the horizontal direction and 11' in the vertical direction. The detector array consists of 80 He-3 detector tubes covering a 160° scattering range. The detectors are position sensitive in the vertical direction with an active length >300 mm. Collimators of 300 mm height and 10' divergence were placed in front of each detector. Diffraction patterns were derived from the two-dimensional data by integration along the Debye-Scherrer rings to achieve high-resolution diffraction data at high intensities.

For the modeling of the background of all patterns, higher order Chebychev polynomials in combination with a $1/2\theta$ term describing the air scattering at low-diffraction angle were employed. The fundamental parameter (FP) approach²⁶ was used to describe the peak profile using direct convolutions of wavelength distribution, the geometry of the diffractometers and microstructural properties such as domain size and strain. Since the geometry of the LynxEye position-sensitive detector is not fully characterized by FPs, fine tuning of the available parameters was performed by using refined values of the FPs from a precise measurement of the NIST line profile standard SRM 660a (LaB_6) measured on a silicon (911) low background sample holder over the full 2θ range of the diffractometer. In case of the neutron data, the wavelength distribution was approximated by a deltalike function due to the lack of a suitable line profile standard. This simplistic approach could *a posteriori* be justified by the fact that the values for the crystallite size came out to be almost identical for the x-ray and the neutron cases. In the neutron powder pattern of the HP phase, several small reflections could be attributed to vanadium which was included in the refinement as a Le Bail fit.²⁷ For structure determination and refinement, the program TOPAS 4.1 (Ref. 28) was used. Indexing of the diffraction data of the HP and R phases was performed by iterative use of singular value decomposition as implemented in TOPAS, leading to a trigonal unit cell for the HP phase and a primitive monoclinic unit cell for the R phase with lattice parameters given in Table I. The most

TABLE I. Crystallographic data for HP-Bi₂O₃ and R-Bi₂O₃. Information from neutron data are given in square brackets.

| Compound | HP-Bi ₂ O ₃ | R-Bi ₂ O ₃ |
|---|--|---|
| Crystallographic data | | |
| Space group | <i>P</i> 31 <i>c</i> (No.159) | <i>P</i> 2 ₁ / <i>c</i> (No. 14) |
| <i>a</i> (Å) | 7.749(1) | 9.107(1) |
| <i>b</i> (Å) | | 7.344(1) |
| <i>c</i> (Å) | 6.302(1) | 10.090(1) |
| β (deg) | | 102.111(1) |
| <i>V</i> (Å ³) | 327.708(1) | 659.805(1) |
| <i>Z</i> | 4 | 8 |
| <i>M_r</i> (g mol ⁻¹) | 465.959 | 465.959 |
| rcalc (g cm ⁻³) | 9.444 | 9.381 |
| Data collection | | |
| Source | Bruker D8 [SPODI] | Bruker D9 [SPODI] |
| Monochromator | Ge(111) [Ge(511)] | Ge(111) [Ge(511)] |
| λ (Å) | Cu <i>K</i> α 1(1.54059) [1.5483] | Cu <i>K</i> α 1(1.54059) [1.5483] |
| 2 θ Range | 10° < 2 θ < 90° [8° < 2 θ < 100°] | 10° < 2 θ < 90° [10° < 2 θ < 150°] |
| Structure refinement | | |
| Program | TOPAS | TOPAS |
| <i>R_{exp}</i> (%) | 2.23 [0.21] | 1.40 [0.22] |
| <i>R_p</i> (%) | 6.10 [2.45] | 6.06 [2.10] |
| <i>R_{wp}</i> (%) | 6.33 [3.23] | 7.11 [2.66] |
| <i>R_{bragg}</i> (%) | 0.63 [2.37] | 2.99 [1.04] |

probable space groups were determined as *P*31*c* and \bar{P} 31*c* for the HP phase and *P*2₁/*c* for the R phase, from the observed extinction rules. From volume increments *Z* was determined to be 4 for the HP and 8 for the R phase. The peak profiles and precise lattice parameters were first determined by Le Bail fits. Structure determinations of both phases were performed by the global optimization method of simulated annealing as implemented in the software.²⁹ The first attempt to solve the crystal structure of the HP phase using x-ray data suggested the presence of a center of symmetry in space group \bar{P} 31*c*. Due to the high-scattering contrast (approximately 100:1) between the strongly scattering bismuth atoms and the much weaker scattering oxygen atoms, the latter could not be located accurately. The plausible crystal structure obtained with two crystallographically independent bismuth atoms showed one undistorted BiO₆ octahedron suggesting the loss of influence of the lone electron pair. A Rietveld refinement of the centrosymmetric crystal structure of the HP phase as derived from the x-ray data did not converge in case of the neutron data. This clearly indicates a violation of the center of symmetry allowing the BiO₆ polyhedron to deviate from a regular octahedron toward a distorted, unilateral widened trigonal antiprism. A change from space group \bar{P} 31*c* to space group *P*31*c* led to immediate

convergence. The crystal structure of the R phase could be directly solved from neutron data without any difficulty with all atoms on general positions.

Combined neutron-x-ray Rietveld refinements³⁰ of the powder patterns of the HP and R phases were performed. During the Rietveld refinement, all crystallographically independent atomic coordinates as well as isotropic temperature factors for the two oxygen atoms and anisotropic temperature factors for the two bismuth atoms were refined. To account for the minor preferred orientation due to the Bragg-Brentano geometry symmetry adapted spherical harmonics of eighth order were introduced. Further corrections were necessary due to a slight specimen displacement error and to account for microabsorption according to surface roughness via the formalism of Pitschke.³¹

C. Crystal-chemical calculations

The stereochemical activity of lone electron pairs can be considered as one of the major causes for the distortion of coordination polyhedra in lone pair bearing compounds. Hence, it is reasonable to consider this distortion for gaining some insights in the stereochemical activity. Various methods have been proposed in literature on how to measure this distortion, such as distortion index,³² quadratic elongation and bond angle variance,³³ or derivatives of the bond valence sum.³⁴ Unfortunately most of them exhibit certain features, which prevent them from being universally applicable. Some of them lead to mathematical discontinuities when the coordination number changes while others are only feasible for certain types of polyhedra. A first approach toward a more universal method for the description of polyhedral distortion and stereochemical activity was proposed by Andersson and Åström¹ and was later improved by Balic Zunic and Makovicky.^{35,36}

The calculation of the centroid or the best center of a polyhedron, its barycenter and crystal-chemical parameters related to the centroid offer multiple options to describe crystallographic distortions. These features are provided by the program IVTON,³⁷ which was used for the crystal-chemical calculations in this work. Among them we consider the volume distortion as a measure for the distortion of a polyhedron. In addition, the projection of the central atom on the centroid—barycenter vector provides a fair, normalized value for the stereochemical activity of the lone electron pairs. Calculations were performed for both structures and the ambient phase as well. For comparison Ag₂₅Bi₃O₁₈ was also included since this mixed-valent compound shows a similar coordination for the Bi^{III} atoms.³⁸ For the Bi^V sites within this compound the expected value for the stereochemical activity is of course zero, due to the absence of a lone electron pair and hence perfectly octahedral coordination.

D. DFT calculations

First-principles DFT calculations have been carried out to investigate the nature of the chemical bond, the stereochemical activity of bismuth lone pairs and the charge transfer between Bi and O in the polymorphs. For comparison, the

ambient phase— α - Bi_2O_3 has also been calculated. The calculations were performed using the Vienna *ab initio* simulation program (VASP),³⁹ applying the projector-augmented wave (PAW) method^{40,41} together with the generalized gradient approximation functional of Perdew-Burke-Ernzerhof.⁴² The PAW potentials present the core electrons of Bi (i.e., $[\text{Xe}] 4f^{14}5d^{10}$ and O $[\text{He}]$) and the energy cutoff for the plane-wave basis was set to 520 eV using a high-precision fast Fourier transform grid. Zone integration was sampled for the Brillouin zone using a $4 \times 4 \times 4$ Monkhorst-Pack k -points mesh. A Gaussian smearing of 0.01 eV was used in all calculations. At first, the experimental crystal structures under investigation were optimized (positions as well as lattice vectors) without any symmetry constraints until the self-consistence convergence of the electronic free energy of 0.1×10^{-6} eV was met and forces on atoms were less than 0.001 eV/Å. The structures were found to retain their crystallographic space groups after the optimizations. These structural optimizations were followed by an additional full relaxation within symmetry and then a static calculation to minimize errors that are associated with the plane-wave basis set incompleteness with respect to the cell volume change during the course of the optimization process.

In order to investigate the bonding properties of HP- Bi_2O_3 and R- Bi_2O_3 versus α - Bi_2O_3 regarding the nature of the chemical bonding, the stereochemical activity of the Bi^{III} lone pair and the charge transfer between Bi and O, analyses of the projected (site and orbital) density of states (PDOS), the electron localization function (ELF) (Ref. 43) and the topology of the charge density⁴⁴ were carried out. The PDOSs were calculated by projecting the wave functions onto spherical harmonics that are nonzero within a Wigner-Seitz sphere radius of 1.68 Å and 1.46 Å for Bi and O ions, respectively. The radius was chosen in such a way that the sum of the volume of the spheres is close to the unit-cell volume and the integration of the electron density over the spheres reproduces the total number of valence electrons. The ELF for all three phases was evaluated from the excess kinetic-energy density due to Pauli repulsion within DFT (Ref. 43) as implemented in VASP. ELF values $\eta(r)$ were normalized between 0 and 1. High ELF values are related to core shells, covalent bonds and lone pairs.

E. Additional investigations

To compliment the results from the DFT calculations and to gain further insight into the properties of the prepared polymorphs, additional investigations with respect to the phase stability and band gap have been performed.

By measuring the diffuse reflectance utilizing a Perkin Elmer Lambda 19 spectrometer, the optical-absorption edge has been determined. Undiluted powder samples were measured through a quartz cuvette (Suprasil) across the visible spectrum with BaSO_4 serving as a reference. In order to be able to determine values for the band gaps the diffuse reflectance spectra first need to be transposed to a corresponding absorption spectrum. The relationship between the absorption and diffuse reflectance of a sample is given by the equation

according to Kubelka and Munk.⁴⁵ The energy scale for the band gap was calculated from the spectroscopic wavelengths according to

$$E(\text{eV}) = \frac{1239.8}{\lambda(\text{nm})}. \quad (1)$$

By applying a tangent to the steepest slope of the absorption curve and extrapolating it to its intersection with the abscissa, the values for the band gap were determined. Phase stability and transformation enthalpy was probed applying both high and low-temperature differential scanning calorimetry (DSC) using a Perkin Elmer Pyris 1 calorimeter across the temperature range -100 °C to 200 °C and Netsch DSC 404 between ambient temperature and 500 °C, respectively. Subsequent calibration/correction of the data was carried out by means of an external sapphire standard.

III. RESULTS AND DISCUSSION

A. Crystal structures

Laboratory x-ray diffraction patterns of the polycrystalline products exhibited reflections in good agreement with those previously reported for a high-pressure modification of Bi_2O_3 .²⁴ However, additional weak reflections could be identified that were not accounted for by the lattice parameters and symmetry reported earlier. The previous authors attributed these to bismuth oxycarbonate impurities. However, careful analysis of the patterns have ruled this out. Furthermore, repeated x-ray diffraction measurements taken at time intervals of weeks revealed that the high-pressure polymorph of Bi_2O_3 (HP- Bi_2O_3) is indeed kinetically unstable at room temperature with a different powder pattern gradually emerging over the course of weeks in each additional sample. Thus for preservation, HP- Bi_2O_3 samples were stored at low temperature ($T = -80$ °C). Annealing HP- Bi_2O_3 samples at mild temperatures ($T = 100$ °C) for periods ranging from days to weeks promoted the formation of the unidentified compo-

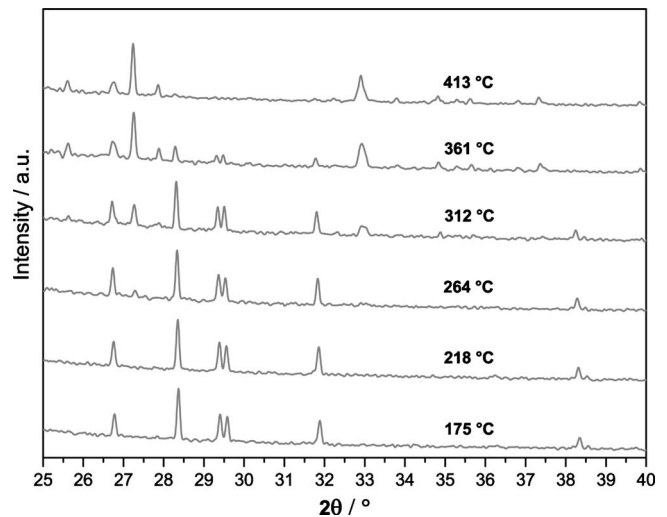


FIG. 1. High-temperature XRD measurements for R- Bi_2O_3 . The transformation to α - Bi_2O_3 starts at 260 °C and is completed at 400 °C.

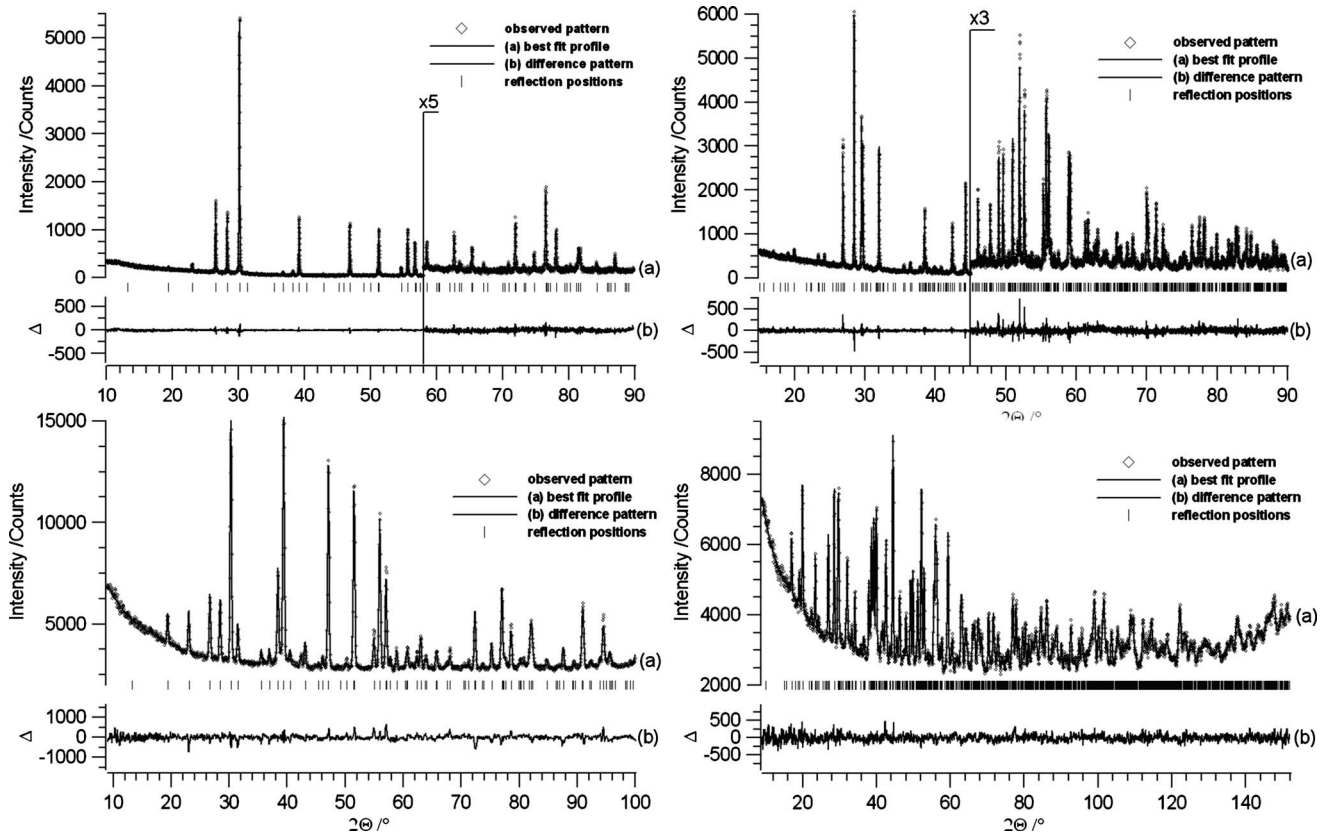


FIG. 2. Scattered x-ray intensities for the HP (left) and R phases (right) of Bi_2O_3 as a function of diffraction angle 2θ for laboratory x ray (top) and neutron (bottom) data. For each are shown the observed pattern (diamonds), the best Rietveld-fit profile (line a), the difference curve between observed and calculated profile (line b), and the reflection markers (vertical bars). The wavelength was $\lambda = 1.54059 \text{ \AA}$ for the x ray and 1.5483 \AA for the neutron data. The higher angle part of the x-ray plots is enlarged by a factor of 5 starting at $58^\circ 2\theta$ for the HP phase and by a factor of 3 starting at $45^\circ 2\theta$ for the R phase, respectively.

ment, until finally the x-ray diffraction patterns no longer exhibited any reflections of HP- Bi_2O_3 . While only the reflections were present that could not be attributed to any previously reported modification of Bi_2O_3 . This modification (R- Bi_2O_3) starts to transform to α - Bi_2O_3 at $260\text{--}270^\circ\text{C}$, with the transition being completed at 400°C (see Fig. 1).

As can be seen in the plotted XRD and neutron patterns in Fig. 2, the refinements converged nicely. The obtained crystallographic data and the final agreement factors (R values) are listed in Table I and the atomic coordinates are given in Table II. Crystallographic data has been deposited at the Fachinformationszentrum (FIZ) Karlsruhe, Hermann-von-Helmholtz-Platz 1, D-76344 Eggenstein-Leopoldshafen, Germany, under CSD 421855 (HP- Bi_2O_3) and CSD 421856 (R- Bi_2O_3) and can be obtained by contacting the FIZ (quoting the article details and the corresponding CSD number).

In turn, the experimental structures were calculated to their equilibrium structure in DFT. The calculated lattice parameters are in fair agreement with the experimental values and given in parenthesis in Table IV. HP- Bi_2O_3 crystallizes in a structure type as shown in Fig. 3. The crystal structure is built from a 3D framework of distorted BiO_6 trigonal antiprisms ($\text{Bi}2$) and heavily distorted BiO_5 square pyramids. Each BiO_5 square pyramid shares one lateral edge and one basal edge with adjacent BiO_5 square pyramids, thus giving rise to infinite chains along the c axis. In turn, each of these

chains is cross-linked to two neighboring chains via corner sharing to yield a bundle at the center of which a threefold axis is located. In turn these bundles are interlinked through the BiO_6 trigonal antiprisms, which are located on the remaining threefold axis and share three of their edges and six corners with the surrounding bundles. Between the bundles there are cavities running along the c axis, separated from

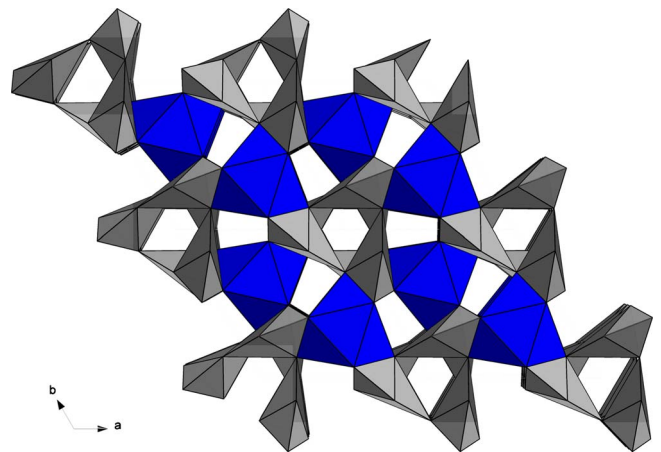


FIG. 3. (Color online) Crystal structure of HP- Bi_2O_3 viewed along $[001]$ with BiO_6 trigonal antiprisms in dark blue and BiO_5 square pyramids in light gray.

TABLE II. Atomic coordinates for HP-Bi₂O₃ (top) and R-Bi₂O₃ (bottom).

| Atom | Site | x | y | z | B (Å ²) |
|------|------|------------|------------|------------|--------------------------|
| Bi1 | 6c | 0.1831(11) | 0.3372(19) | 0.2291(40) | 0 |
| Bi2 | 2b | 2/3 | 1/3 | 1/4 | 0 |
| O1 | 6c | 0.39(23) | 0.451(25) | 0.963(35) | 7.13(10) |
| O2 | 6c | 0.851(23) | 0.718(24) | 0.167(15) | 6.848(77) |
| Bi1 | 4e | 0.291(1) | 0.9059(5) | 0.9286(5) | 0.416(13) |
| Bi2 | 4e | 0.9167(4) | 0.4017(6) | 0.3174(4) | 0.416(13) |
| Bi3 | 4e | 0.4306(5) | 0.1266(6) | 0.3369(3) | 0.416(13) |
| Bi4 | 4e | 0.2057(6) | 0.3823(5) | 0.0679(5) | 0.416(13) |
| O1 | 4e | 0.4289(1) | 0.3667(1) | 0.1737(1) | 0.962(20) |
| O2 | 4e | 0.9205(1) | 0.3462(1) | 0.5286(1) | 0.962(20) |
| O3 | 4e | 0.712(1) | 0.955(1) | 0.839(0) | 0.962(20) |
| O4 | 4e | 0.2242(1) | 0.194(1) | 0.888(1) | 0.962(20) |
| O5 | 4e | 0.287(1) | 0.942(1) | 0.427(1) | 0.962(20) |
| O6 | 4e | 0.1938(11) | 0.8605(3) | 0.7197(1) | 0.962(20) |

one another by the BiO₆ octahedra. In particular, these octahedra exhibit a structural feature, which requires a detailed analysis. Only two different Bi-O distances are present, three short bonds (at 2.350 Å) on one side and three somewhat longer bonds (at 2.635 Å) on the other side, which leads to a widened triangular face. A similar coordination for trivalent bismuth is known to occur in Ag₂₅Bi₃O₁₈.³⁸ Since the oxygen atoms perfectly obey the symmetry around the trigonal axis and do not exhibit any further distortion, one might speculate about a decreased stereochemical activity of the electron lone pair based on geometric consideration. In contrast to HP-Bi₂O₃, in the relaxed modification R-Bi₂O₃ we find a 3D crystal structure built exclusively from corner/edge sharing distorted BiO₅ square pyramids (see Fig. 4), with four distinct bismuth sites being present. R-Bi₂O₃ shows some similarities to α-Bi₂O₃, which is stable at ambient conditions. Like the latter it is also built up from corner-/edge-sharing square pyramids and also crystallizes in space group $P2_1/c$ but with twice the unit-cell volume. In fact, it can be

considered as an intermediate modification, occurring only during the back transformation of the high pressure toward the ambient phase. Any attempt to directly synthesize R-Bi₂O₃ by high-pressure and high-temperature experiments with α-Bi₂O₃ proved to be futile. A flow chart of the structural changes during backtransformation (for sake of clarity only Bi positions) is given in Fig. 5. The trigonal 120° feature, originating from the initial hexagonal close packing (hcp), becomes more and more distorted, until it completely vanishes within the monoclinic ambient modification. The original A and B layer of the hcp stacking evolve different during the phase transformations, as can be seen in the graphical depiction.

Crystal-chemical parameters obtained from calculations utilizing the program IVTON are listed in Table III. As can be seen in the graphical representation of the polyhedral distortion (i.e., volume distortion) calculated according to Makovicky *et al.*³⁶ in Fig. 6, the lowest value when considering only the Bi₂O₃ modifications is actually obtained for the

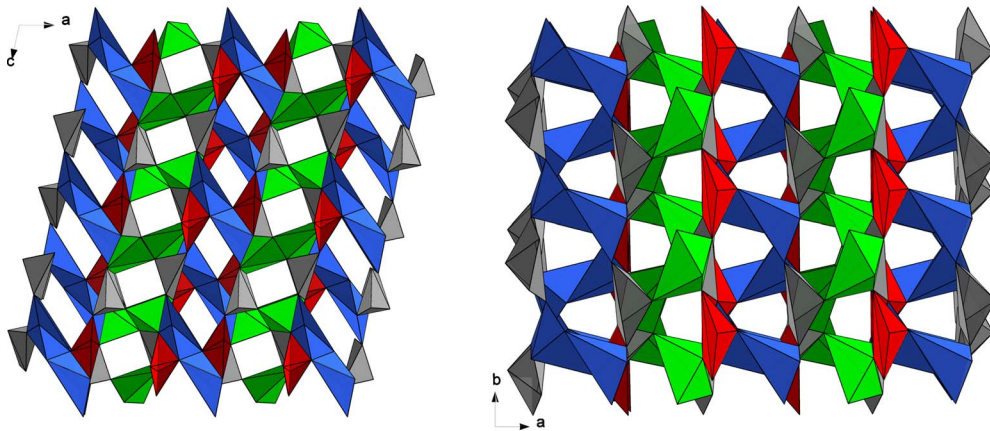


FIG. 4. (Color online) Crystal structure of R-Bi₂O₃ viewed along the [010] (left side) and [001] (right side). The BiO₅ square pyramids are displayed in red (Bi1), blue (Bi2), green (Bi3), and gray (Bi4) for distinction.

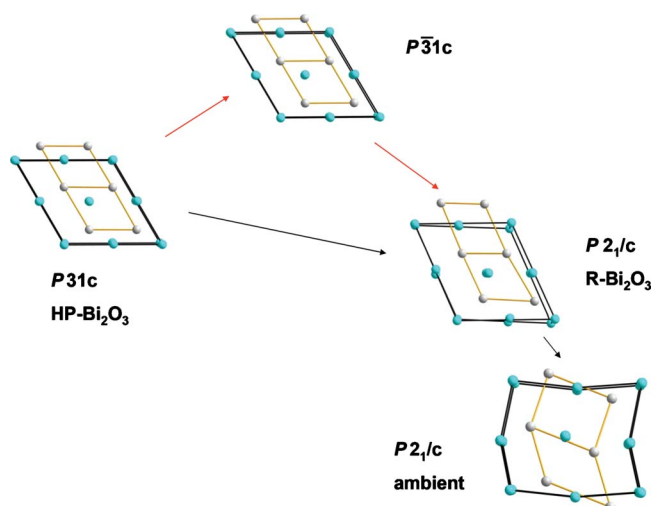


FIG. 5. (Color online) Structural variation in Bi_2O_3 polymorphs during transformation toward the stable at ambient conditions α phase. The bismuth atoms are divided into the individual A and B layers of the original hexagonal close packing, which are found to evolve different upon phase transformation. A hypothetical, ideal centrosymmetric structure without stereochemically active lone pairs (top) is given for comparison.

Bi 2*b* site of HP- Bi_2O_3 . A similar plot is obtained for the normalized projection of the central atom on the vector centroid barycenter (which we suggest as a reasonable means of quantifying the degree of stereochemical activity). The lowest value within the polymorphs is again obtained for the high symmetric Bi 2*b* site of HP- Bi_2O_3 . Hence, by applying high pressure and following stabilization of the phase post-experiment, the stereochemical activity of one bismuth lone electron pair has been reduced. As expected for pentavalent bismuth in $\text{Ag}_{25}\text{Bi}_3\text{O}_{18}$, the IVTON analysis suggests zero stereochemical activity for the absent lone pair. Structural voids such as observed in the graphical representation of the crystal structures in Figs. 3 and 4 are in general considered to host the lone electron pairs. However, this issue can be affirmed if the displacement of the central atom to the centroid is assumed to be opposite to the orientation of the lone pair as proposed earlier.¹ According to the crystal-chemical calculations presented in this work, it is possible to locate the lone pairs into the structural voids of the bismuth oxide polymorphs. Thus, in R- Bi_2O_3 a two-dimensional network of tubes (along [010] and [001] directions), filled with lone pairs, results (see Fig. 4).

On the other hand, in HP- Bi_2O_3 four lone-pairs point into common voids, respectively. Three of them originate from bismuth atoms (Bi1) on equivalent crystallographic sites, perfectly aligned around a threefold axis and with dipole moments compensating each other. The fourth lone pair is associated with the bismuth atom on the special 2*b* position and points in the $[00\bar{1}]$ direction. Since there is no lone pair left to countervail the latter, a polar structure is formed in the high-pressure polymorph.

B. Phase stability

From the computed binding energies listed in Table IV it is evident that HP- Bi_2O_3 is thermodynamically less stable

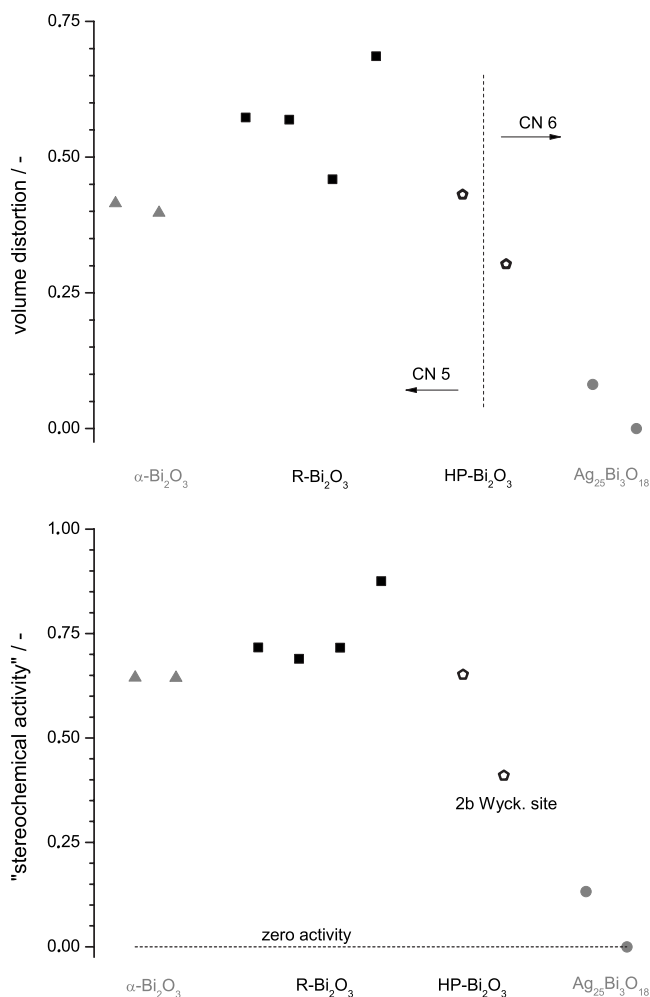


FIG. 6. Top: volume distortion of the distinct Bi polyhedra within the polymorphs. For comparison also α - Bi_2O_3 and the mixed-valent compound $\text{Ag}_{25}\text{Bi}_3\text{O}_{18}$ are depicted. Bottom: projection of the central atom on the barycenter-centroid vector as a normalized measure of stereochemical activity or inertness of the lone pairs.

than R- Bi_2O_3 by $11.10 \text{ kJ mol}^{-1}$. This is supported by our experimental DSC observations where an exothermic (9.6 kJ mol^{-1}) reconstructive first-order phase transition was observed to occur from the HP to the R polymorph (Fig. 7). By repeated measurements applying different heating rates (10 – 65 K min^{-1}) and extrapolation to 0 K , the onset of the transformation was determined to $106 \text{ }^\circ\text{C}$.

No DSC signal was detected for the transition of R- Bi_2O_3 to the ambient phase, although according to the calculated values, the intermediate R- Bi_2O_3 to be an intermediate distorted variant of the ambient phase, this energy cost could be attributed to the local distortions. Following the DSC measurements of R- Bi_2O_3 , powder x-ray patterns were remeasured for the specimens. Despite the absence of any visible DSC peak, the samples were confirmed to have completely transformed back to pure α - Bi_2O_3 . From the graphic representation of high-temperature XRD measurements shown in Fig. 1, the transition is known to range from 260 to $400 \text{ }^\circ\text{C}$. This

TABLE III. Lone-pair stereochemical activity results from crystal-chemical calculations.

| Compound | Atom/center | Coordinates | | | Volume distortion | Normalized projection | | |
|--|--|-----------------------------------|------------|------------|-------------------|-----------------------|--------|--------|
| | | <i>x</i> | <i>y</i> | <i>z</i> | | | | |
| α -Bi ₂ O ₃ | Bi1 | 0.5227(4) | 0.1837(3) | 0.3615(3) | 0.4147 | 0.6448 | | |
| | Centroid | 0.4961 | 0.2246 | 0.3838 | | | | |
| | Barycenter | 0.5579 | 0.1095 | 0.4084 | | | | |
| | R-Bi ₂ O ₃ | Bi2 | 0.0401(3) | 0.0426(3) | 0.7762(3) | 0.3976 | 0.6441 | |
| | | Centroid | 0.0707 | 0.0811 | 0.7753 | | | |
| | | Barycenter | -0.0536 | 0.0161 | 0.7979 | | | |
| R-Bi ₂ O ₃ | | Bi1 | 0.291(1) | 0.9059(5) | 0.9286(5) | 0.5732 | 0.7165 | |
| | | Centroid | 0.3537 | 0.8929 | 0.9587 | | | |
| | | Barycenter | 0.2128 | 0.9005 | 0.9338 | | | |
| | HP-Bi ₂ O ₃ | Bi2 | 0.9167(4) | 0.4017(6) | 0.3174(4) | 0.5688 | 0.6897 | |
| | | Centroid | 0.9667 | 0.4291 | 0.2739 | | | |
| | | Barycenter | 0.8480 | 0.4256 | 0.3380 | | | |
| | | HP-Bi ₂ O ₃ | Bi3 | 0.4306(5) | 0.1266(6) | 0.3369(3) | 0.4594 | 0.7162 |
| | | | Centroid | 0.4552 | 0.1580 | 0.3602 | | |
| | | | Barycenter | 0.3579 | 0.1058 | 0.2955 | | |
| | HP-Bi ₂ O ₃ | | Bi4 | 0.2057(6) | 0.3823(5) | 0.0679(5) | 0.6861 | 0.8758 |
| | | | Centroid | 0.1637 | 0.3483 | 0.0795 | | |
| | | | Barycenter | 0.2826 | 0.3611 | 0.0257 | | |
| HP-Bi ₂ O ₃ | | Bi1 | 0.1831(11) | 0.3372(19) | 0.2291(40) | 0.4312 | 0.6514 | |
| | | Centroid | 0.1874 | 0.3730 | 0.2850 | | | |
| | | Barycenter | 0.2246 | 0.2810 | 0.2854 | | | |
| | Ag ₂₅ Bi ₃ O ₁₈ | Bi2 | 2/3 | 1/3 | 1/4 | 0.303 | 0.4096 | |
| | | Centroid | 2/3 | 1/3 | 0.1896 | | | |
| | | Barycenter | 2/3 | 1/3 | 0.3150 | | | |
| Ag ₂₅ Bi ₃ O ₁₈ | | Bi1 | 1/3 | 2/3 | 0.2393(1) | 0.0812 | 0.1318 | |
| | | Centroid | 1/3 | 2/3 | 0.1929 | | | |
| | | Barycenter | 1/3 | 2/3 | 0.2604 | | | |
| (No lone pair) | Bi2 | 0 | 0 | 1/2 | 0.0003 | 0 | | |
| | Centroid | 0 | 0 | 1/2 | | | | |
| | Barycenter | 0 | 0 | 1/2 | | | | |

suggests that the R-Bi₂O₃ to α -Bi₂O₃ transition exhibits comparatively slower kinetics (such that the thermal effect may be smeared out and thus evades detection).

C. Electronic structure

The diffuse reflectance spectra (Fig. 8) show the electronic similarity of α - and R-Bi₂O₃ with band gaps of 2.74 eV and 2.78 eV, respectively. In contrast, the band gap of HP-Bi₂O₃ is significantly reduced to 2.48 eV. Although the absolute values deviate, the same trend can be seen in the DFT results (2.00 eV, 2.06 eV, and 1.55 eV, respectively).

In all three phases the PDOS (Fig. 9) are quite similar and can be divided into three manifolds of bands. The low-energy band around -17 eV is narrow and it corresponds to the O(2s) orbital. In the energy range between -10.4 to -7.8 the bands possess mainly Bi(6s) and to a less extent O(2p) character. These bands represent the lone pairs. The bands between -5 to 0 eV (the Fermi energy level, E_f) are mostly

constructed from O(2p) and Bi(6p) orbitals. Close to E_f (between -2 to 0 eV) some Bi(6s) contributions are apparent. Although the electronic energy dispersion spectra of the three polymorphs look rather alike, a minor but obvious difference can be seen in the site specific Bi(6s) PDOS (Fig. 10) of HP and α -Bi₂O₃ (since α -Bi₂O₃ is known we have used it for comparison here). The band with 6s character for the six-coordinate Bi site (Bi2) in HP-Bi₂O₃ is relatively lower in energy compared to the band associated with the five-coordinate Bi (Bi1 in HP, Bi1 and Bi2 in α -Bi₂O₃).

To finally examine the stereochemical activity we have calculated the ELF which can be related to concepts of chemical bonding and is known to be one of the primary tools to probe the shape of electron lone pairs in direct space. The topology of the ELF shows maxima on Bi atoms at $\eta \sim 1$. In Fig. 11, we show ELF isosurface domains for the three phases of Bi₂O₃ at $\eta=0.96$. The ELF maxima close to the Bi atoms at $\eta \sim 1$ can be regarded as Bi electron lone pairs. The ELF domains on the Bi atoms point into the voids

TABLE IV. Crystallographic data, binding and relative energies (BE, RE) for HP-Bi₂O₃, R-Bi₂O₃, and α -Bi₂O₃. Comparison between experimental and calculated (parenthesis) values.

| Compound | HP-Bi ₂ O ₃ | R-Bi ₂ O ₃ | α -Bi ₂ O ₃ ^a |
|---|-----------------------------------|------------------------------------|---|
| Space group | <i>P</i> 31 <i>c</i> | <i>P</i> 2 ₁ / <i>c</i> | <i>P</i> 2 ₁ / <i>c</i> |
| <i>a</i> (Å) | 7.749 (7.888) | 9.107 (9.423) | 5.844 (5.931) |
| <i>b</i> (Å) | 7.749 (7.888) | 7.344 (7.373) | 8.157 (8.282) |
| <i>c</i> (Å) | 6.302 (6.159) | 10.090 (10.325) | 7.503 (7.518) |
| β (deg) | | 102.11 (103.14) | 112.97 (112.32) |
| <i>V</i> (Å ³) | 327.71 (331.87) | 659.80 (698.52) | 329.35 (341.64) |
| <i>Z</i> | 4 | 8 | 4 |
| BE/Bi ₂ O ₃ (eV) | -28.532 | -28.647 | -28.762 |
| RE w.r.t. | 0.00 | -9.60 | |
| HP-Bi ₂ O ₃ (kJ mol ⁻¹) | (0.00) | (-11.10) | (-22.26) |

^aReference 46.

or tunnels of the lattice, thus showing the same geometrical arrangement as deduced from the crystal-chemical calculations. In HP-Bi₂O₃, the lone pairs on Bi1 lie roughly in the *ab* plane while on Bi2 they run along the *c* axis. This resultant directionality (polarity) of the electron lone pair induces an electric dipole moment in the crystal consistent with the noncentrosymmetric space group. The overall shape of the ELF domains at the Bi atoms is aspherical, suggesting a slight hybridization of the Bi 6*s* and Bi 6*p* orbitals. In the PDOS plots such a hybridization can only be seen in the energy range between 2 eV and E_f (Fig. 9), as also noticed by Watson and co-workers.⁴⁷ As the bands between -10.4 and -7.8 eV, where no Bi(6*p*) contributions are found, are associated to the lone pairs, the asphericity and thus the stereochemical activity can only come from an admixture of O(2*p*) orbitals which also contribute to the bands near the

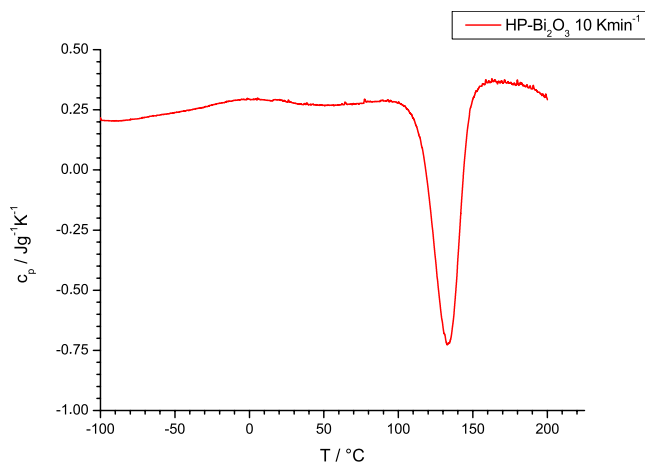


FIG. 7. (Color online) Calibrated DSC measurement for HP-Bi₂O₃. A heating rate of 10 K min⁻¹ was applied.

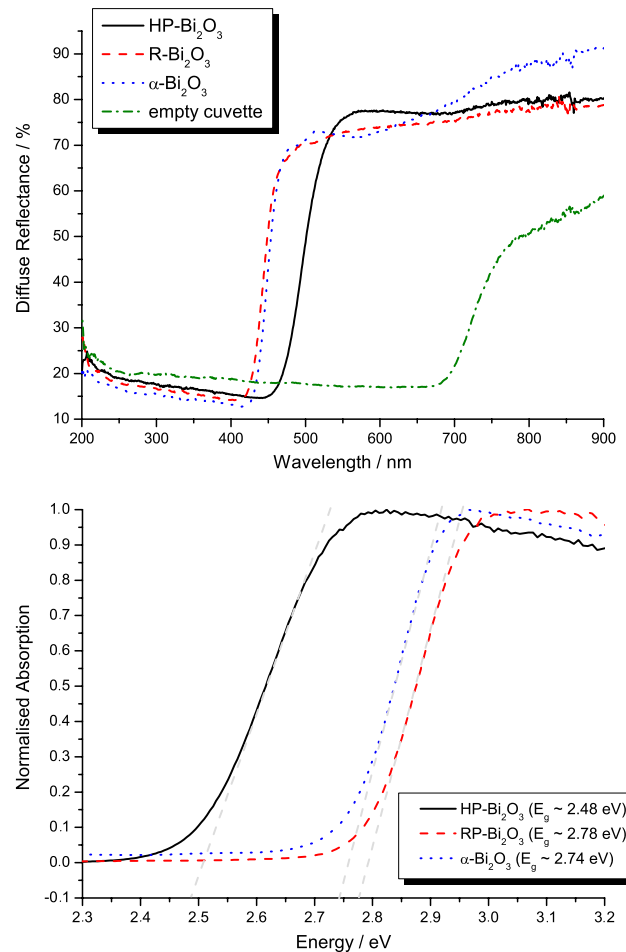


FIG. 8. (Color online) Observed diffuse reflection spectra for HP-Bi₂O₃, R-Bi₂O₃, and α -Bi₂O₃ from 200 to 900 nm (top) and corresponding optical-absorption energies (bottom) calculated from the Kubelka Munk formula.

Fermi level. The stereochemical activity thus can be regarded as ligand induced. The degree of the asphericity of the ELF domains on Bi2 in the HP phase is fairly reduced in

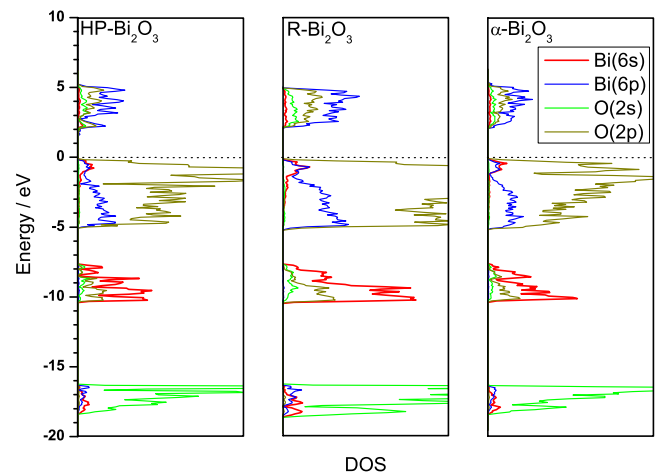


FIG. 9. (Color online) Projected DOSs for HP-, R-, and α -Bi₂O₃ phases. The dashed line at 0 eV indicates the position of the Fermi level.

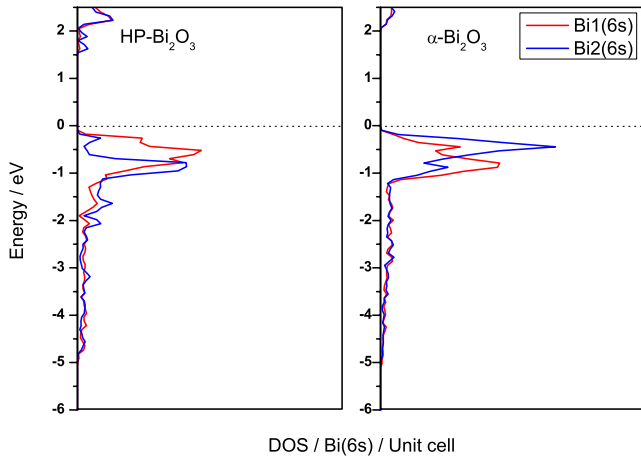


FIG. 10. (Color online) Site-specific projected DOS of Bi(6s) for HP- and α -Bi₂O₃ phases.

comparison to other Bi sites as shown in Fig. 11. This can be related to the lowering of bands with Bi2(6s) character at the Fermi level in the HP phase as mentioned above, which leads to a modified mediation via the ligands and consequently to an enhanced *s* character of the lone pair. In the ELF attractors can be found that might be related to covalent bonds. All attractors starting at $\eta=0.96$ on Bi and $\eta=0.86$ on O belong to the atomic sites. The corresponding domains merge at $\eta=0.58$ (not shown in Fig. 11).

One can propose the Bi₂O₃ phases to be predominantly ionic in nature. In order to quantify the charge transfer between Bi and O, we have calculated partial charges from the converged electron density obtained with VASP using a grid based Bader topological charge analysis.⁴⁸ The computed Bader partial charges for HP-, R-, and α -Bi₂O₃ are tabulated in Table V. The partial charges are rather similar in the various phases and differ slightly on the various crystallographically independent sites (designated by the Wyckoff positions in Table V) due to asymmetry in the coordination polyhedron or local geometric distortion. For the fivefold coordinated Bi

TABLE V. Bader partial charges.

| Atom | Wyckoff position | Partial charge |
|---|------------------|----------------|
| HP-Bi ₂ O ₃ (trigonal— <i>P31c</i>) | | |
| Bi1 | 6 <i>c</i> | 1.701 |
| Bi2 | 2 <i>b</i> | 1.623 |
| O1 | 6 <i>c</i> | -1.133 |
| O2 | 6 <i>c</i> | -1.109 |
| R-Bi ₂ O ₃ (monoclinic— <i>P2₁/c</i>) | | |
| Bi1 | 4 <i>e</i> | 1.649 |
| Bi2 | 4 <i>e</i> | 1.706 |
| Bi3 | 4 <i>e</i> | 1.684 |
| Bi4 | 4 <i>e</i> | 1.693 |
| O1 | 4 <i>e</i> | -1.126 |
| O2 | 4 <i>e</i> | -1.092 |
| O3 | 4 <i>e</i> | -1.102 |
| O4 | 4 <i>e</i> | -1.152 |
| O5 | 4 <i>e</i> | -1.135 |
| O6 | 4 <i>e</i> | -1.124 |
| α -Bi ₂ O ₃ (monoclinic— <i>P2₁/c</i>) | | |
| Bi1 | 4 <i>e</i> | 1.676 |
| Bi2 | 4 <i>e</i> | 1.711 |
| O1 | 4 <i>e</i> | -1.142 |
| O2 | 4 <i>e</i> | -1.128 |
| O3 | 4 <i>e</i> | -1.117 |

atoms the charges vary by less than 3%. On the average 1.7 electrons are transferred from Bi to O gaining a charge of -1.1. Such partial charges agree well with the formal oxidation state of +3 for Bi and -2 for O. The Bi2 in the HP-Bi₂O₃ phase has 5% less charge in comparison to the Bi1 site despite the higher coordination number. The reduced charge transfer can be related to the reduced mediation via

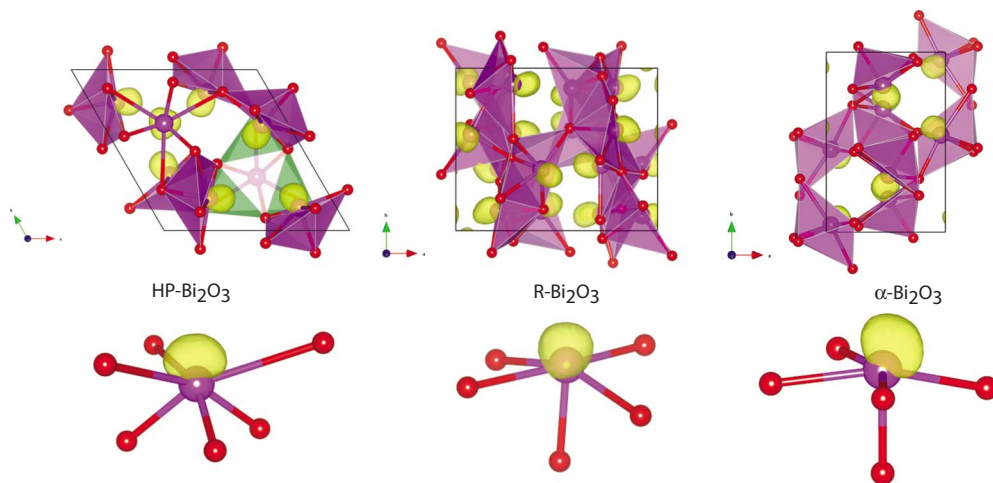


FIG. 11. (Color online) Domains of the ELF, $\eta=0.96$, in HP-, R-, and α -Bi₂O₃ phases. The lone pairs of Bi2 in HP-, Bi1 in R- and α -Bi₂O₃ are shown below their respective phases. The Bi1 site in HP-Bi₂O₃ and the rest of the Bi sites in R- and α -Bi₂O₃ are not shown as they are similar to Bi1 lone pairs.

the ligand atoms. In the HP phase the lone pair is still stereochemically active, as implied by the distorted sixfold coordinate site. However, all structural and electronic data point to a diminishing of the effect.

IV. CONCLUSION

We were able to synthesize two polymorphs within the family of Bi_2O_3 modifications by high-pressure and high-temperature multianvil experiments. Crystal structures were determined by combined Rietveld refinement from x-ray and neutron-diffraction powder data. The high-pressure polymorph of Bi_2O_3 crystallizes in an additional structure type. It transforms back toward $\alpha\text{-Bi}_2\text{O}_3$ via relaxation of the constrained Bi-O bonds via an intermediate step, in which R- Bi_2O_3 is formed. The metastable behavior of the HP and R phase over $\alpha\text{-Bi}_2\text{O}_3$ was investigated and confirmed by *in situ* high-temperature x-ray diffraction and DSC and the results were supported by thermodynamic calculations. The band gap was found to be decrease significantly within

HP- Bi_2O_3 whereas it remains similar to $\alpha\text{-Bi}_2\text{O}_3$ in the R phase. Furthermore, due to crystal-chemical and DFT calculations we were able to prove that the stereochemical activity of the lone electron pairs of specific Bi sites was significantly reduced. Another feature of the noncentrosymmetric HP- Bi_2O_3 is the uncompensated polarization of the Bi^{3+} lone electron pairs. Thus, in its high-pressure modification Bi_2O_3 can be considered as a ferroelectric. To gain more insight into ferroelectricity, structural behavior at nonambient conditions and other properties, DFT calculations as well as further experiments are currently in progress.

ACKNOWLEDGMENTS

The authors would like to thank Frank Falkenberg (for assistance with the multianvil experiments), Wolfgang Koenig (for UV-Vis.-NIR measurements), and Ewald Schmitt (for DSC measurements). The financial support of the DFG, in particular, the SPP 1236, and the Fonds der Chemischen Industrie (FCI) is gratefully acknowledged.

-
- ¹S. Andersson and A. Åström, *Solid State Chemistry*, Proceedings of the Fifth Materials Research Symposium Vol. 364 (NBS Spec., Gaithersburg, MD, 1972), pp. 3–14.
- ²I. D. Brown, *J. Solid State Chem.* **11**, 214 (1974).
- ³J. Galy, G. Meunier, S. Andersson, and A. Åström, *J. Solid State Chem.* **13**, 142 (1975).
- ⁴A. Leclaire, J. Chardon, J. Provost, and B. Raveau, *J. Solid State Chem.* **163**, 308 (2002).
- ⁵J. P. Laval, L. Guillet, and B. Frit, *Solid State Sci.* **4**, 549 (2002).
- ⁶L. Nistor, G. Van Tendeloo, S. Amelinckx, V. Kahlenberg, and H. Böhm, *J. Solid State Chem.* **119**, 281 (1995).
- ⁷J. C. Champarnaud-Mesjard, S. Blanchandin, P. Thomas, A. Mirgorodsky, T. Merle-Méjean, and B. Frit, *J. Phys. Chem. Solids* **61**, 1499 (2000).
- ⁸X. Wang, F. X. Zhang, I. Loa, K. Syassen, M. Hanfland, and Y.-L. Mathis, *Phys. Status Solidi B* **241**, 3168 (2004).
- ⁹D. M. Adams, A. G. Christy, J. Haines, and S. M. Clark, *Phys. Rev. B* **46**, 11358 (1992).
- ¹⁰J.-M. Raulot, G. Baldinozzi, R. Seshadri, and P. Cortona, *Solid State Sci.* **4**, 467 (2002).
- ¹¹H. Giefers and F. Porsch, *Physica B* **400**, 53 (2007).
- ¹²R. E. Dinnebier, S. Carlson, M. Hanfland, and M. Jansen, *Am. Mineral.* **88**, 996 (2003).
- ¹³U. Häussermann, P. Berastegui, S. Carlson, J. Haines, and J.-M. Léger, *Angew. Chem., Int. Ed.* **40**, 4624 (2001).
- ¹⁴D. Becker and H. P. Beck, *Z. Kristallogr.* **219**, 348 (2004).
- ¹⁵H. J. Terpstra, R. A. De Groot, and C. Haas, *J. Phys. Chem. Solids* **58**, 561 (1997).
- ¹⁶M. B. Robin and P. Day, *Adv. Inorg. Chem. Radiochem.* **10**, 247 (1968).
- ¹⁷D. Orosel, O. Leynaud, P. Balog, and M. Jansen, *J. Solid State Chem.* **177**, 1631 (2004).
- ¹⁸L. G. Sillen, *Z. Kristallogr.* **103**, 274 (1941).
- ¹⁹A. Laarif and F. Theobald, *Solid State Ionics* **21**, 183 (1986).
- ²⁰H. A. Harwig, *Z. Anorg. Allg. Chem.* **444**, 151 (1978).
- ²¹N. Cornei, N. Tancret, F. Abraham, and O. Mentre, *Inorg. Chem.* **45**, 4886 (2006).
- ²²A. F. Gualtieri, S. Immovilli, and M. Prudenziati, *Powder Diffr.* **12**, 90 (1997).
- ²³C. Chouinard and S. Desgreniers, *Solid State Commun.* **113**, 125 (1999).
- ²⁴T. Atou, H. Faqir, M. Kikuchi, H. Chiba, and Y. Syono, *Mater. Res. Bull.* **33**, 289 (1998).
- ²⁵M. Hoelzel, A. Senyshyn, R. Gilles, H. Boysen, and H. Fuess, *Neutron News* **18**, 23 (2007).
- ²⁶R. W. Cheary, A. A. Coelho, and J. P. Cline, *J. Res. Natl. Inst. Stand. Technol.* **109**, 1 (2004).
- ²⁷A. Le Bail, H. Duroy, and J. L. Fourquet, *Mater. Res. Bull.* **23**, 447 (1988).
- ²⁸A. A. Coelho, *J. Appl. Crystallogr.* **36**, 86 (2003).
- ²⁹A. A. Coelho, *J. Appl. Crystallogr.* **33**, 899 (2000).
- ³⁰H. M. Rietveld, *J. Appl. Crystallogr.* **2**, 65 (1969).
- ³¹W. Pitschke, N. Mattern, and H. Hermann, *Powder Diffr.* **8**, 223 (1993).
- ³²W. H. Baur, *Acta Crystallogr., Sect. B: Struct. Crystallogr. Cryst. Chem.* **30**, 1195 (1974).
- ³³K. Robinson, G. V. Gibbs, and P. H. Ribbe, *Science* **172**, 567 (1971).
- ³⁴I. D. Brown, *Acta Crystallogr., Sect. B: Struct. Sci.* **62**, 692 (2006).
- ³⁵T. Balic Zunic and E. Makovicky, *Acta Crystallogr., Sect. B: Struct. Sci.* **52**, 78 (1996).
- ³⁶E. Makovicky and T. Balic Zunic, *Acta Crystallogr., Sect. B: Struct. Sci.* **54**, 766 (1998).
- ³⁷T. Balic Zunic and I. Vickovic, *J. Appl. Crystallogr.* **29**, 305 (1996).
- ³⁸M. Bortz and M. Jansen, *Angew. Chem.* **103**, 841 (1991).
- ³⁹G. Kresse and J. Furthmüller, *Phys. Rev. B* **54**, 11169 (1996).
- ⁴⁰P. E. Blöchl, *Phys. Rev. B* **50**, 17953 (1994).
- ⁴¹G. Kresse and D. Joubert, *Phys. Rev. B* **59**, 1758 (1999).

- ⁴²J. P. Perdew, K. Burke, and M. Ernzerhof, *Phys. Rev. Lett.* **77**, 3865 (1996).
- ⁴³A. Savin, O. Jepsen, J. Flad, O. K. Andersen, H. Preuß, and H. G. von Schnering, *Angew. Chem.* **104**, 186 (1992); *Angew. Chem., Int. Ed. Engl.* **31**, 187 (1992).
- ⁴⁴R. F. W. Bader, *Atoms in Molecules: A Quantum Theorie* (Oxford University Press, Oxford, 1994).
- ⁴⁵P. Kubelka and F. Munk, *Z. Tech. Phys. (Leipzig)* **12**, 593 (1931).
- ⁴⁶S. A. Ivanov, R. Tellgren, H. Rundlof, and V. G. Orlov, *Powder Diffr.* **16**, 227 (2001).
- ⁴⁷A. Walsh, G. W. Watson, D. J. Payne, R. G. Edgell, J. Guo, P. A. Glans, T. Learmonth, and K. E. Smith, *Phys. Rev. B* **73**, 235104 (2006).
- ⁴⁸W. Tang, E. Sanville, and G. Henkelman, *J. Phys.: Condens. Matter* **21**, 084204 (2009).